

CIRCULATION COPY

**SUBJECT TO BE
IN TWO WEEKS**

**A SYNCHROTRON RADIATION BEAM LINE FOR PHOTONS
IN THE 700 eV - 7000 eV ENERGY RANGE**

**P. J. Ebert
C. J. Anderson**

APRIL 1, 1985

**Lawrence
Livermore
National
Laboratory**

This is an informal report intended primarily for internal or limited external distribution. The opinions and conclusions stated are those of the author and may or may not be those of the Laboratory.

Work performed under the auspices of the U.S. Department of Energy by the Lawrence Livermore Laboratory under Contract W-7405-Eng-48.

DISCLAIMER

This document was prepared as an account of work sponsored by an agency of the United States Government. Neither the United States Government nor the University of California nor any of their employees, makes any warranty, express or implied, or assumes any legal liability or responsibility for the accuracy, completeness, or usefulness of any information, apparatus, product, or process disclosed, or represents that its use would not infringe privately owned rights. Reference herein to any specific commercial products, process, or service by trade name, trademark, manufacturer, or otherwise, does not necessarily constitute or imply its endorsement, recommendation, or favoring by the United States Government or the University of California. The views and opinions of authors expressed herein do not necessarily state or reflect those of the United States Government or the University of California, and shall not be used for advertising or product endorsement purposes.

Printed in the United States of America
Available from
National Technical Information Service
U.S. Department of Commerce
5285 Port Royal Road
Springfield, VA 22161
Price: Printed Copy \$; Microfiche \$4.50

<u>Page Range</u>	<u>Domestic Price</u>	<u>Page Range</u>	<u>Domestic Price</u>
001-025	\$ 7.00	326-350	\$ 26.50
026-050	8.50	351-375	28.00
051-075	10.00	376-400	29.50
076-100	11.50	401-426	31.00
101-125	13.00	427-450	32.50
126-150	14.50	451-475	34.00
151-175	16.00	476-500	35.50
176-200	17.50	501-525	37.00
201-225	19.00	526-550	38.50
226-250	20.50	551-575	40.00
251-275	22.00	576-600	41.50
276-300	23.50	601-up ¹	
301-325	25.00		

¹Add 1.50 for each additional 25 page increment, or portion thereof from 601 pages up.

**A SYNCHROTRON RADIATION BEAM LINE FOR PHOTONS
IN THE 700 eV - 7000 eV ENERGY RANGE**

P. J. Ebert and C. J. Anderson

ABSTRACT

The design of a beam line for synchrotron radiation research is described. The 700-7000 eV energy range to be covered is determined at low energy by the 2d spacing of easily obtainable diffraction crystals and at high energy by the cutoff of specular reflection of a Pt mirror. Two mirrors are used, the first to collimate the x-ray beam through a double crystal monochromator and the second to focus the collimated monochromatic beam on target. In this way, high monochromatic x-ray throughput is achieved with energy resolution limited by crystal diffraction properties.

April 1, 1985

**A SYNCHROTRON RADIATION BEAM LINE FOR PHOTONS
IN THE 700 eV - 7000 eV ENERGY RANGE**

P. J. Ebert and C. J. Anderson

I. INTRODUCTION

Beam line VIII-B is one of two beam lines under construction at SSRL by LLNL for the UC-National Laboratories Proposal Research Team (PRT). Because of the diversity of scientific interests within the PRT, each beam line should cover a large energy range with high resolution, high throughput and with a well defined, small spot on target.

BL VIII-B has ~20 mrad of useful horizontal arc available for the synchrotron radiation (SR) emanating from the bending magnet. Of these, 12 mrad are for a VUV branch that will cover the 5 eV to 180 eV energy interval, 1 mrad is for an electron beam position monitor branch that allows control of the vertical position of the x-ray beam by steering the stored electron beam, 5 mrad are for the soft x-ray (SXR) branch that is the subject of this report and 2 mrad are for space between the three branches (see Fig. 1). The SXR branch will provide photons in the 700 eV to 7000 eV energy range using easily obtainable diffraction crystals. With synthetic multi-layers, it is possible to obtain lower energy photons (~100 to ~500 eV), but with poorer energy resolution. Organic crystals also diffract low energy photons, but most have limited utility in intense x-ray beams.

The SXR branch was placed on the bend magnet line instead of the wiggler for two reasons: a) it can be accomplished at substantially lower cost;

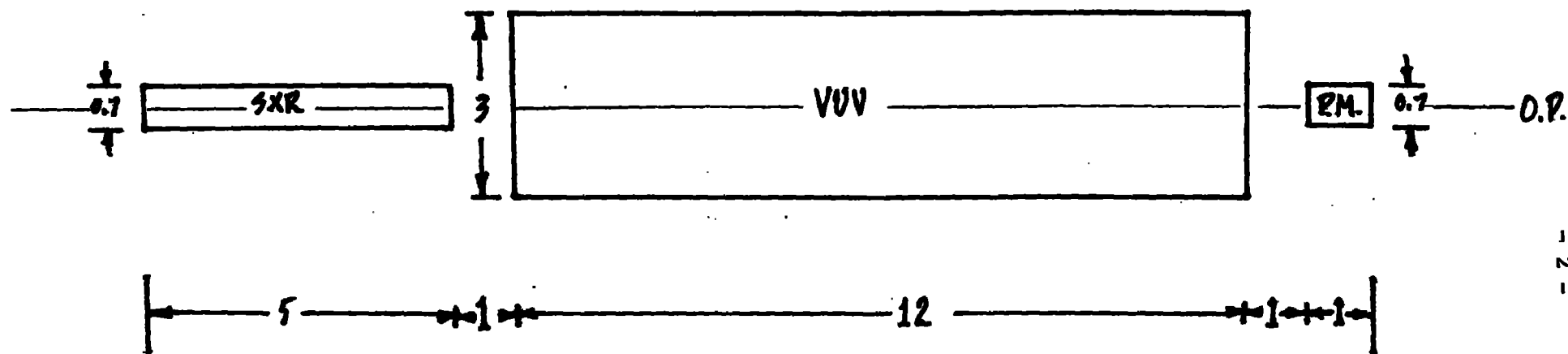


FIG. 1. BEAM LINE VIII-B ANGLE BUDGET.

DRAWING IS APPROXIMATELY TO SCALE AT A DISTANCE OF 10m FROM THE X-RAY SOURCE. THIS VIEWS THE SPACE ALLOCATION FROM THE SOURCE. ALL DIMENSIONS ARE IN MILLIRADIANS. P.M. = POSITION MONITOR. THE ORBITAL PLANE (O.P.) IS ALSO SHOWN.

b) the number of photons available for experimentation from the bend magnet is within a factor of 2 of the number from the wiggler because a wiggler SXR branch would require several reflections of less than 1 deg to have enough lateral space for both soft and hard x-ray experiment stations. Cerino, et al [Nucl. Instrum. and Meth. 172, 227 (1980).] have described the design of a similar beam line at SSRL, and Hussain, et al [Nucl. Instrum. and Meth. 195, 115 (1982)] have described its performance.

To have a useful SXR beam line several key components are required. These are schematically illustrated in Fig. 2, which also includes valves, shutters, pumps, etc. needed for personnel and equipment safety. Not shown are upstream components common to both the VUV and SXR branch lines and also required for operations and safety. Thus, only those components necessary for scientific performance will be discussed. A mask assures that the x-ray beam shines upon only the desired optical component, namely the first mirror, which provides a low energy bandpass and also collimates the x-ray beam vertically and horizontally. Vertical collimation matches the beam divergence with the rocking curves of the diffraction crystals, thereby increasing x-ray throughput. Horizontal collimation reduces size requirements for downstream components. A filter may be necessary to reduce the VUV flux on the first crystal of the monochromator, and with proper choices of material and thickness, effectively absorb lower order diffraction peaks. Thus, heat, VUV radiation damage, and spectral content can be controlled. The monochromator provides crystal-limited energy resolution above ~ 700 eV. Possible crystals are β -alumina, mica, synthetic mica, InSb, Ge and Si; α -SiO₂ can also be useful with low x-ray fluxes. To extend to lower energy, synthetic multilayers must be used unless organic crystals that are stable in SR and ultra-

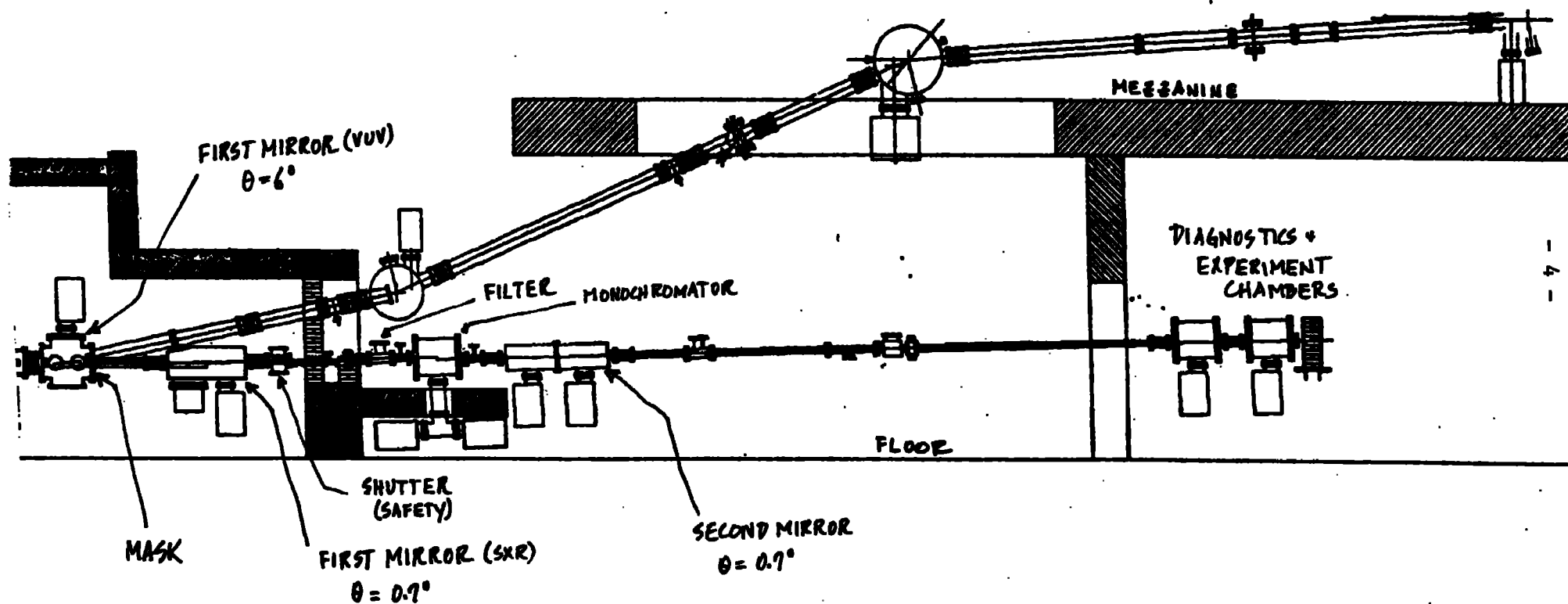


FIG. 2 SCHEMATIC DIAGRAM OF B.L. VIII-B SHOWING BOTH THE VUV AND SXR BRANCHES.
NOT SHOWN ARE SEVERAL UPSTREAM SAFETY COMPONENTS AND THE POSITION MONITOR.

high vacuum can be found. Of all these, mica, synthetic mica, Ge, Si and multilayers seem appropriate for the SXR branch. The second mirror focuses the monochromatized x-rays on the sample. This mirror will be identical to the first mirror in order to reduce costs. A chamber(s) is provided for beam monitoring and experiments. Relevant beam parameters include photon energy, photon throughput (photons/sec.), beam spot size, photon flux, time structure, degree of polarization and higher order beam contamination. Some, but probably not all of these beam measurements will be required for each experiment.

Whether high energy resolution, high throughput and a well defined target spot can be obtained depends in large measure on the design of the beam line components as well as on the operating conditions of the storage ring. Handling SR beam power is a major consideration. The SR power absorbed can be high enough to heat sensitive beam line components to temperatures where performance is significantly degraded. Thus it is important to have reliable estimates for thermal loading of critical components such as mirrors and crystals. Other equally practical considerations deal with locating beam line components, availability of components and the tradeoffs between availability, performance, utility and cost. In general, the latter considerations will be implicit in the discussion that follows.

II. PROPERTIES OF SYNCHROTRON RADIATION

When a charged particle is accelerated, it emits radiation that is characterized by the energy of the particle and the nature of the acceleration. If the acceleration is normal to the instantaneous velocity vector of a highly relativistic particle the motion is circular and the radiation is called synchrotron radiation. In high energy electron storage rings such as SPEAR at Stanford, synchrotron radiation is emitted in a narrow beam parallel to the instantaneous velocity vector as the electrons respond to the transverse force while traveling through the magnetic field of each bending magnet. Synchrotron radiation exhibits several important properties including high intensity, broad spectral range, a high degree of linear polarization, pulsed time structure and natural collimation in the orbital plane of the stored electrons. Synchrotron radiation can be reflected and focused to experimental targets with a variety of optical elements such as grazing incidence mirrors or synthetic multilayers. Gratings, diffraction crystals and synthetic multilayers provide monoenergetic photon beams that are variable over specific energy ranges of the synchrotron spectrum. For general references, the reader should consult Synchrotron Radiation Research, H. Winick and S. Doniach, Eds. and Synchrotron Radiation, Techniques and Applications, C. Kunz, Editor.

The SR power per horizontal milliradian emitted during magnetic deflection is given by

$$\begin{aligned} \frac{dP}{d\omega_H} &= 4.22 \text{ BE}^3 \text{I} \frac{W}{\text{mr}} && \text{B-Tesla} \quad \text{E-GeV, I-A} \\ &= 14.1 \text{ E}^4 \frac{I}{R} \frac{W}{\text{mr}} && \text{R-m} \end{aligned} \tag{1}$$

where E is the electron energy, I the time averaged beam current, B the magnetic field strength and R the radius of curvature. For any bend magnet beam line, the x-rays are emitted from an arc source of length $L_s = R \Delta\omega_H$ where $\Delta\omega_H$ is the angular width of the beam line. For our beam line, $R = 12.7\text{m}$ and $\Delta\omega_H = 5 \times 10^{-3}\text{rad}$. Thus $L_s = 63.5\text{mm}$. The x-ray energy flux normally incident on a target located at a distance Z from the source center is given approximately by

$$\frac{dP}{dA} = \frac{dP}{d\omega_H} \cdot \frac{E \times 10^6}{Z^2} \frac{W}{\text{cm}^2} ; \quad Z - \text{cm} \quad (2)$$

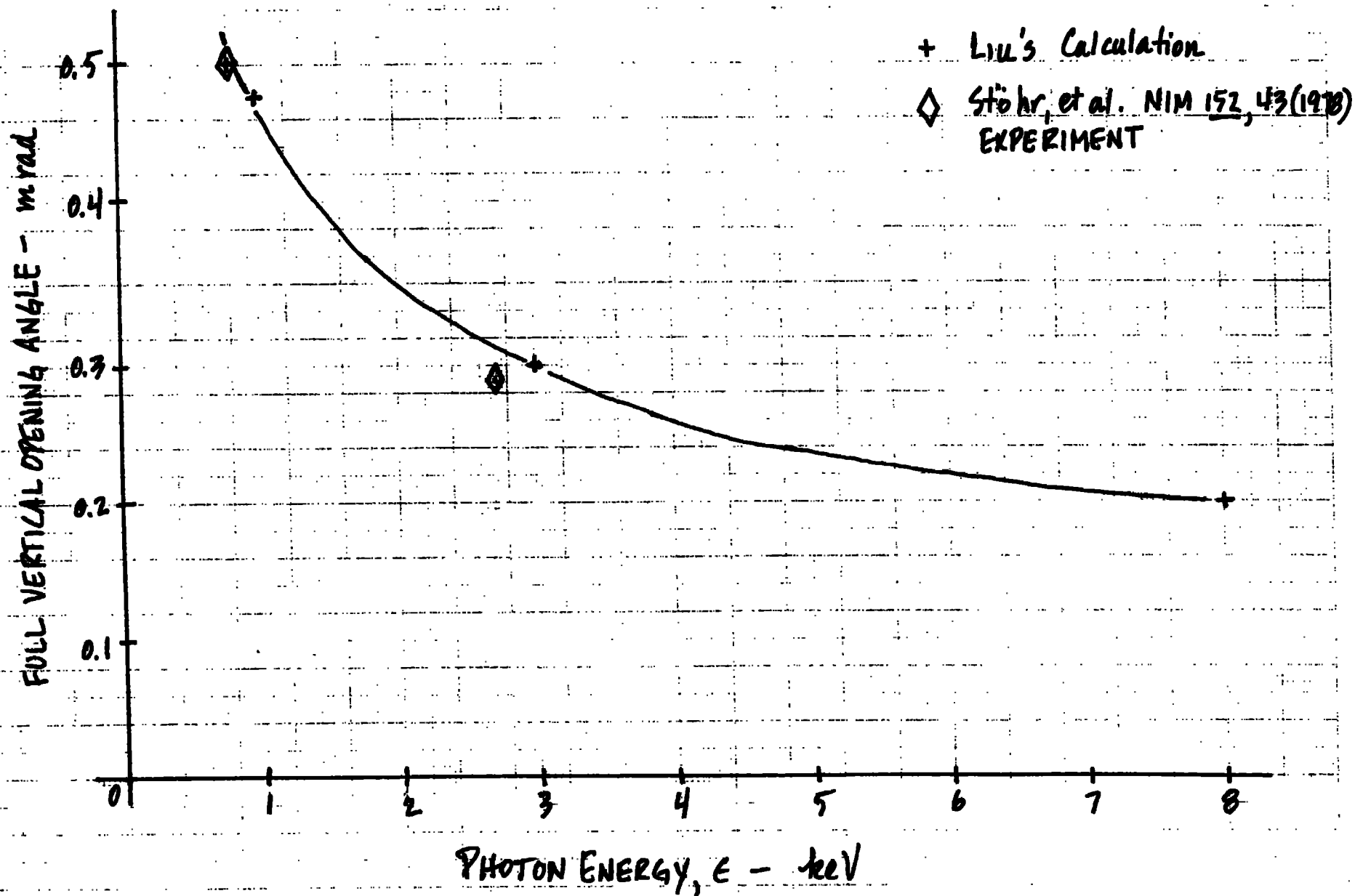
To obtain Eq. 2, we must make note that the vertical distribution of the beam is approximately Gaussian with a $1/e$ width of $\omega_v = 1/E \text{ mr}$. The vertical opening angle is a function of both the electron beam energy and the photon energy.

Figure 3 is a plot of the vertical opening angle as a function of photon energy at 3 GeV that was calculated by R. Liu of SSRL. The measured values at 800 eV and 2700 eV are in close agreement. To estimate heat loading however, $\omega_v = 1/E$ is a reasonable approximation. Within this vertical angle, the SR beam is highly polarized in the orbital plane (horizontally).

The SR critical energy ϵ_c (half the emitted energy is above ϵ_c) is given by

$$\epsilon_c = 2.22 \frac{E^2}{R} = 0.665BE^2 \text{ keV} \quad (3)$$

FIG. 3 VERTICAL OPENING ANGLE VS. PHOTON ENERGY @ 3 GeV .



Since R is fixed, the magnetic field is adjusted to obtain the desired electron energy. In Fig. 4 we plot the normalized integral power spectrum versus normalized photon energy ϵ/ϵ_c . Table I lists values of $\frac{1}{I} \frac{dP}{d\omega_H}$, $\frac{1}{I} \frac{dP}{dA}$, and ϵ_c for several stored energies. Also listed are values of $\frac{dP}{dA}$ for the usual dedicated operating conditions at SSRL of 3.0 GeV, 100mA and 3.4 GeV, 60mA. While the energy fluxes are comparable for these two cases the higher beam energy gives rise to a harder x-ray spectrum. Fig. 5 shows SR spectra produced at 2,3 and 3.4 GeV. It should be noted that all such curves have the same shape when plotted on logarithmic graph paper.

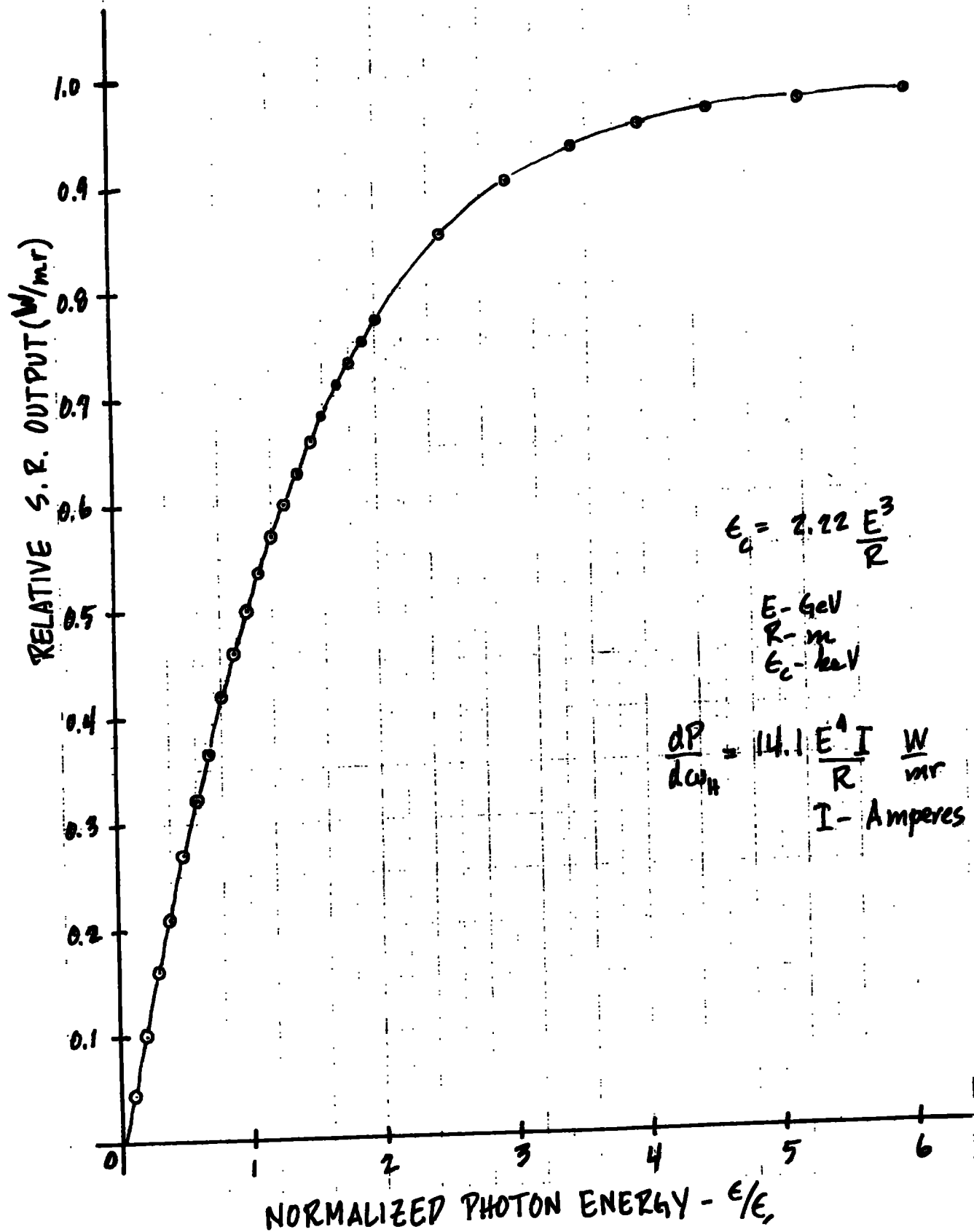
TABLE I
SPEAR OPERATING PARAMETERS

E - GeV	$\frac{1}{I} \frac{dP}{d\omega_H} \frac{W}{mr-mA}$	$\frac{1}{I} \frac{dP}{dA} (10 \text{ cm}) \frac{W}{cm^2-mA}$	$\epsilon_c - \text{keV}$	Total Flux @ 10m w/cm ²
2.0	0.018	0.035	1.4	3.5 (a)
2.5	0.043	0.11	2.7	10.5 (a)
3.0	0.090	0.26	4.7	26 (a)
3.4	0.15	0.49	6.9	30 (b)
3.7	0.21	0.76	8.9	46 (b)

(a) 100 mA stored current

(b) 60 mA stored current

FIG. 4-5. R. INTEGRAL \bar{P}^{10} SPECTRUM



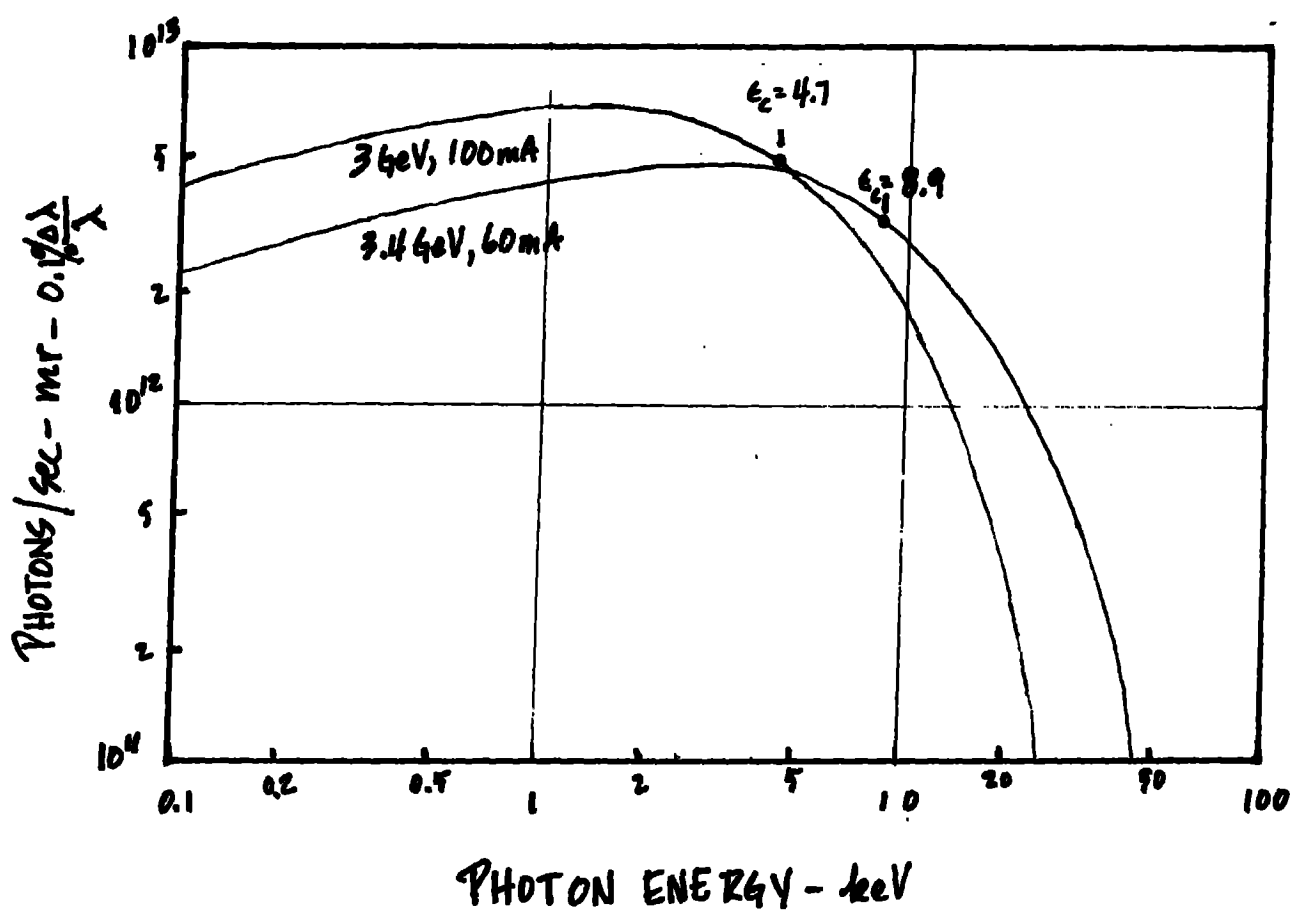


FIG. 5 SYNCHROTRON RADIATION SPECTRA AT
3 AND 3.4 GeV.

III. Beam Line Components

This section describes the function, location and parameters needed for each key component.

A. First Mask. This element defines the horizontal and vertical dimensions of the SXR beam. The mask will be located in the VUV mirror chamber at a distance of $Z = 8.8$ m from the center of the electron beam arc defining the SR source for this branch line. The horizontal and vertical dimensions are 4.4 cm (5 mr) and 0.62 cm (0.7 mr), respectively. The latter is slightly larger than the 0.5 mr needed to allow for variation in the vertical position of the stored electron beam. At 8.8 m from the source, the average flux is ~ 40 W/cm²; therefore water cooling is required. The mask is of OFHC copper construction and is opaque to x-rays.

B. First Mirror. The mirror serves two functions, (a) to define a high energy cutoff for the beam line and (b) to efficiently collect and collimate the divergent x-ray beam. To allow adequate distance for separating the VUV and SXR branches, the center of the mirror will be at $Z = 10.0$ m. At this location, the flux is 30 W/cm².

It is desirable to have both a high energy cutoff and collimation on this branch in order to avoid severely degrading the performance of the crystal monochromator. Without both a cutoff and collimation, thermal loading would be higher than necessary, rejection of higher order diffraction peaks much more difficult to accomplish and x-ray throughput much lower. This is relatively straightforward to accomplish by exploiting the x-ray reflectivity of highly polished surfaces at grazing angles of incidence. This is routinely

done at SR facilities with bent concave quartz cylinders which have a very thin ($\sim 1000 \text{ \AA}$) metallic overcoating to enhance small angle reflectivity. We have chosen Pt for the overcoating because it has high x-ray reflectivity and is very stable. The calculated reflectivity of Pt as a function of photon energy is plotted for several angles of incidence in Fig. 6. For smaller angles of incidence, θ , both the cutoff energy and reflectivity increase. However, the smaller the angle, the longer the mirror must be. This behavior is shown in Fig. 7. The angle selected was $0.7 \text{ deg} = 12.2 \text{ mr}$ to keep the mirror length reasonably short, yet provide adequate x-ray flux below $\sim 7 \text{ keV}$.

The beam incident on the mirror is divergent both horizontally and vertically. Since crystal diffraction plane is vertical (parallel to the plane of polarization) it is important to collimate vertically so that the divergence of the beam matches the rocking curve widths of available diffraction crystals. In this way the need for vertical slits to improve energy resolution is relaxed. Horizontal collimation is necessary to keep the beam width to a reasonable size. Otherwise it would be difficult to diffract and efficiently collect photons further downstream for focusing to a small, well-defined spot on target. A schematic diagram of the x-ray optic chosen is shown in Fig. 8.

For small incidence angles a cylinder bent to a large meridional radius of curvature (toroid) is a close approximation to the required paraboloidal figure necessary for collimation. See J. A. Howell and P. Horowitz, Nucl. Instrum. and Meth. 125, 225 (1975) and S. M. Heald and J. B. Hastings, Nucl. Instrum. and Meth. 187, 553 (1981) for reference. The mirror radii required were obtained using the treatment of Heald and Hastings. The sagittal radius

FIG 6. REFLECTIVITY OF Pt VS. ENERGY

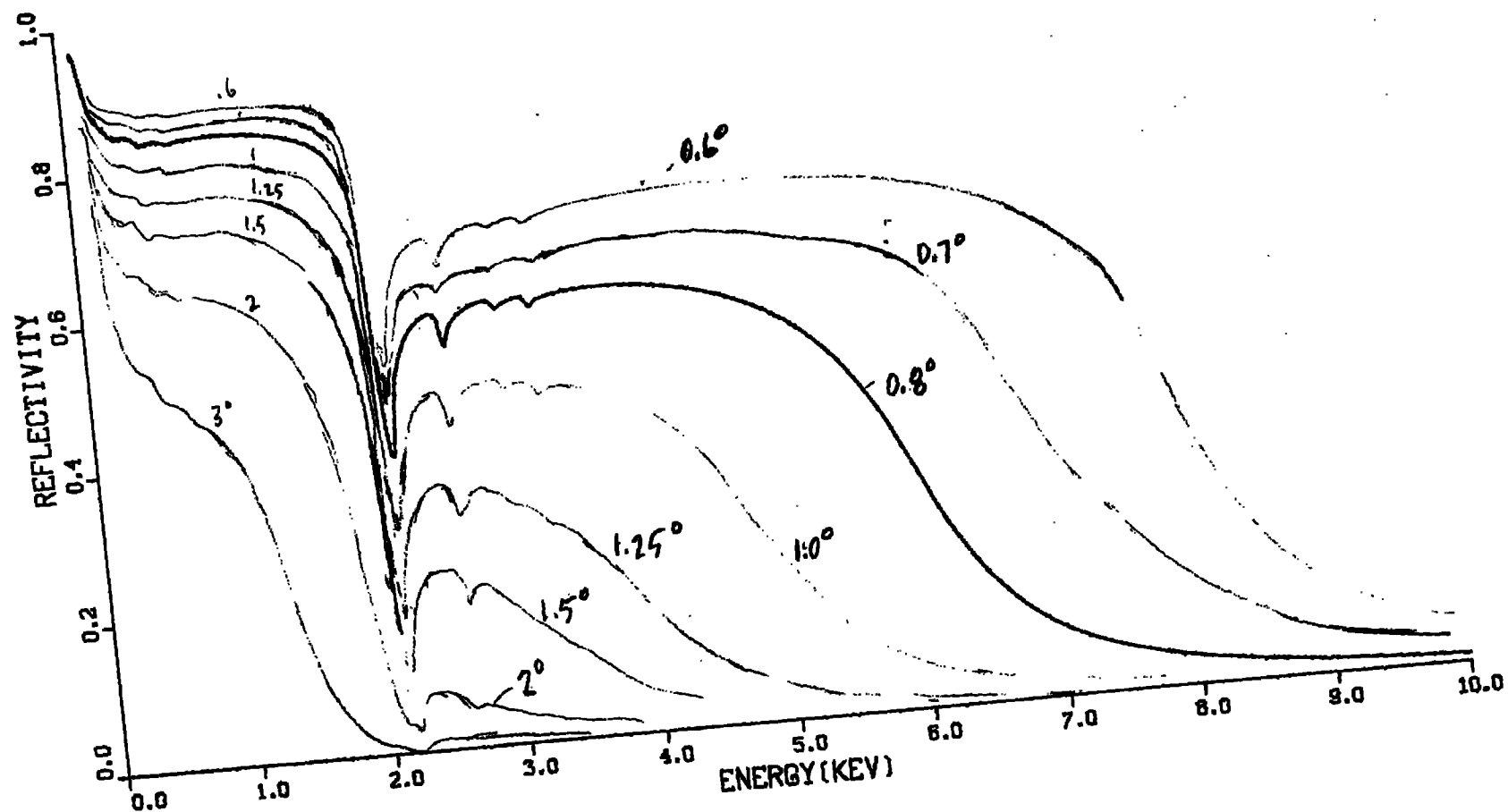
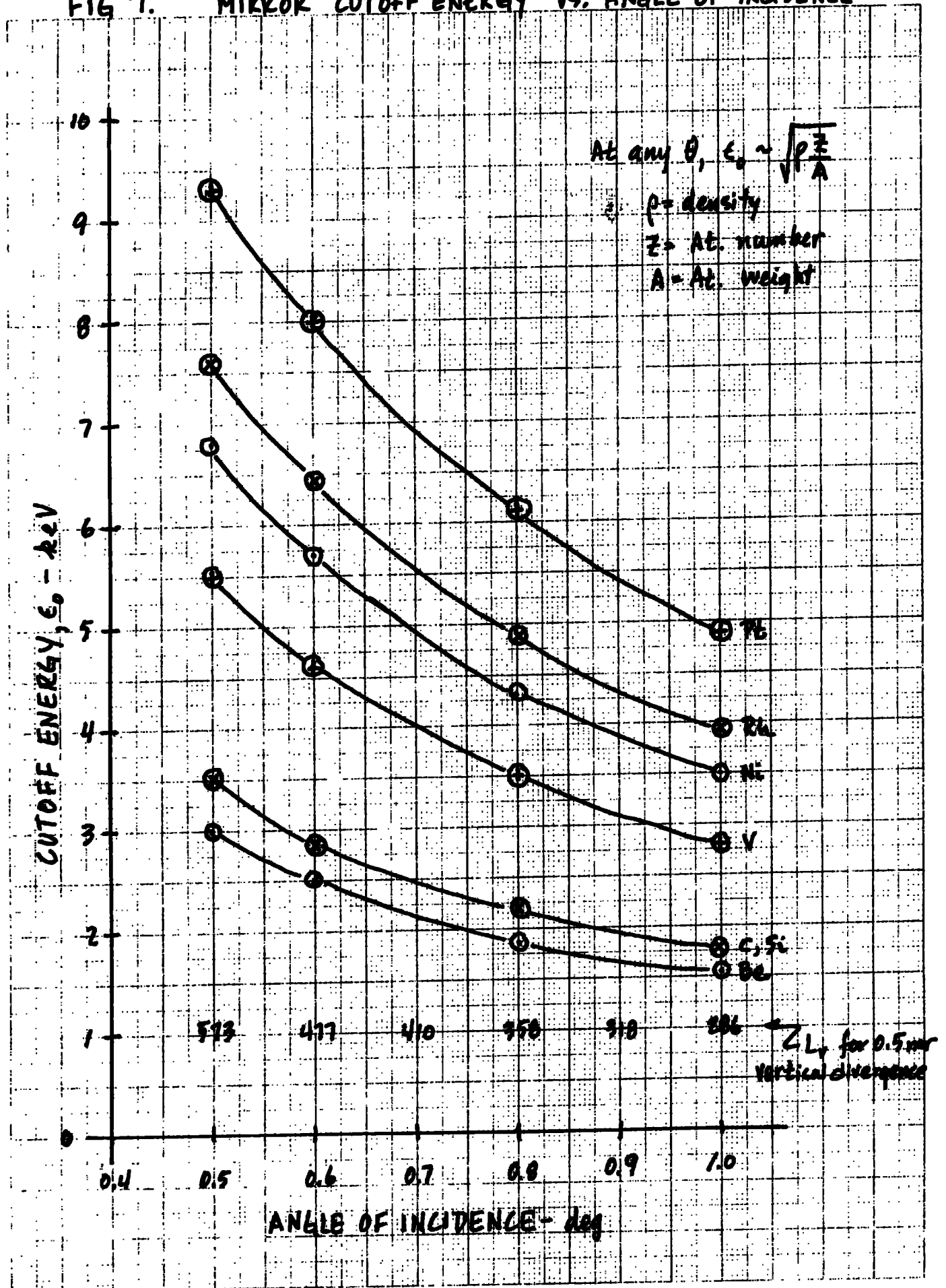


FIG 7. MIRROR CUTOFF ENERGY VS. ANGLE OF INCIDENCE



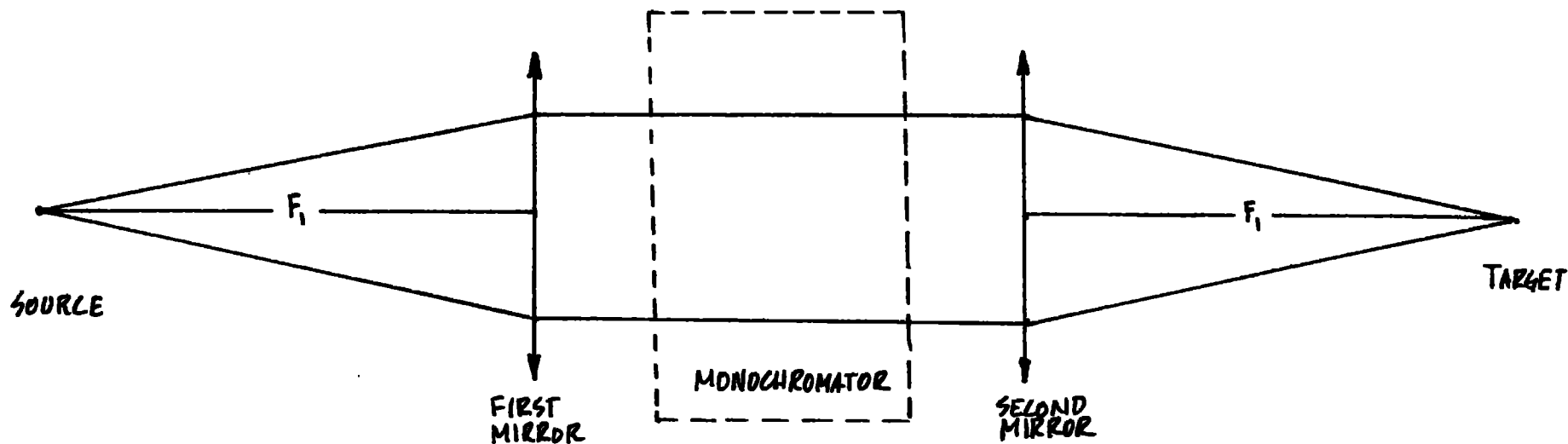


FIG. 8 SCHEMATIC DIAGRAM OF THE X-RAY OPTICS. THE FIRST MIRROR CONVERGES THE BEAM TO MATCH THE ANGULAR ACCEPTANCE OF THE MONOCHROMATOR. THE SECOND MIRROR CONVERGES THE BEAM ON TARGET. THIS SYSTEM HAS UNIT MAGNIFICATION. $F_1 = 10.0\text{m}$. CONVERGENCE IS BOTH VERTICAL AND HORIZONTAL.

of curvature, R_s , (see Fig. 9) is given by

$$R_s = \frac{2F_1 F_2}{F_1 + F_2} \sin \theta \quad (4)$$

where F_1 is the source to mirror distance, F_2 the mirror to image distance and θ is the angle of incidence. The meridional radius of curvature, R_m , is given by

$$R_m = \frac{2F_1 F_2}{F_1 + F_2} \cdot \frac{1}{\sin \theta} = \frac{R_s}{\sin^2 \theta} \quad (5)$$

Curvature in the sagittal or transverse dimension gives horizontal focusing or collimation, while meridional or longitudinal curvature gives vertical focusing or collimation. To collimate vertically, we set $F_2 = \infty$ in (4) and obtain

$$R_s = 2 F_1 \sin \theta \quad ; \quad R_m = 2F_1 / \sin \theta \quad (6 \text{ a,b})$$

Now the length L of the mirror needed to collect both horizontal and vertical divergence can be expressed as

$$L = L_v + L_H \quad (7)$$

where L_v is the "vertical" mirror length to intercept photons spread vertically and L_H is the "horizontal" mirror length that is needed to collimate photons horizontally.* These terms are given by

*Another way of understanding the L_H term is that an amount of mirror equal to $\Delta_s / \sin \theta$, where Δ_s is the sagittal depth, must be added to collect the full horizontal fan. In the small angle approximation, $\Delta_s = (F_1 \omega_H)^2 / 8 R_s$. (See Fig. 9).

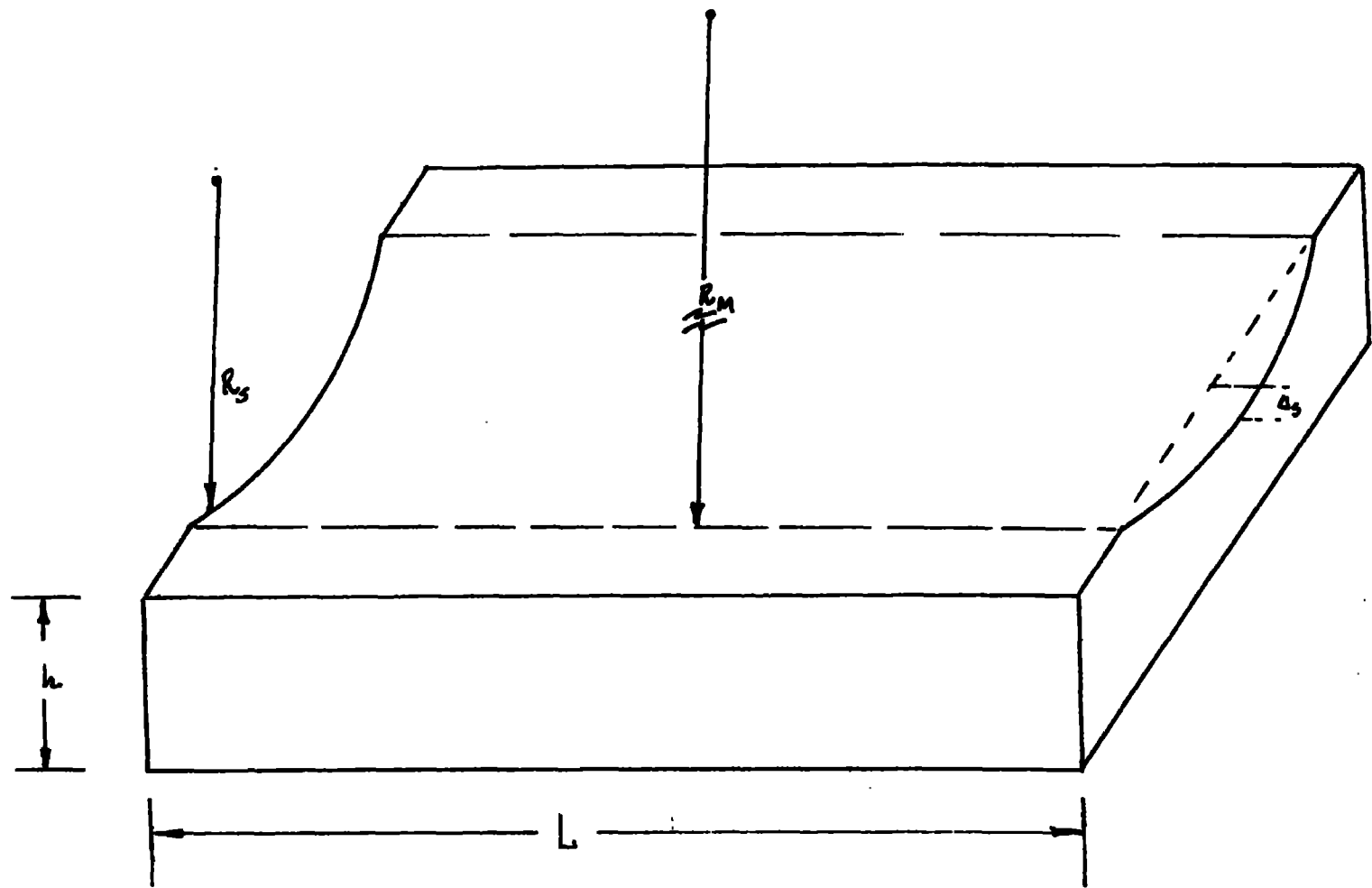


FIG. 9 SCHEMATIC DIAGRAM OF CONVERGING MIRROR. THE SAGITTAL RADIUS, R_s , IS GROUND INTO THE QUARTZ. THE MERIDIONAL RADIUS, R_m , IS OBTAINED BY MECHANICAL BENDING.

$$L_V = \omega_V F_1 / \sin \theta \quad (8)$$

and

$$L_H = \frac{\omega_H^2 F_1}{16 \theta^2 + \omega_H^2} \quad (9)$$

where ω_V and ω_H are the vertical and horizontal beam divergences, respectively. Note that when $\omega_H \ll \theta$ that $L_H \sim \omega_H^2 F_1$. For the SXR branch, $\omega_V = 0.5$ mr, $\omega_H = 5$ mr, $\theta = 0.7$ deg = 12.22 mr and $F_1 = 10.0$ m. Using these values, we obtain, from equations 5 through 9 the following: $R_S = 0.244$ m, $R_m = 1636$ m, $L_V = 0.41$ m, $L_H = 0.10$ m and $L = 0.51$ m. A highly polished mirror with these specifications is relatively inexpensive and easy to obtain.

A question yet to be addressed is whether this mirror will reduce the vertical divergence sufficiently to match the rocking curves of diffraction crystals. Equations 4 to 9 were derived assuming a point source of x-rays. Since the stored electron beam has finite dimensions ($S_H = 4 \times 10^{-3}$ m, $S_V = 0.56 \times 10^{-3}$ m) the focusing will be imperfect. This is manifested by an additional spread in vertical angle after reflection. Just as for the length of the mirror, there are two contributions to this. The first term which arises from the vertical extent of the electron beam is analogous to the penumbra obtained with an aperture and is given by the expression

$$\delta\theta_V = S_V / F_1 \quad (10)$$

The second term arises because different parabolic paths are traced on the mirror surface by the divergent photon beams that emanate from horizontally separated source points. This contribution is given approximately by

$$\delta \theta_p = \frac{S_H \omega_H}{2F_1 \theta} \quad . \quad (11)$$

These contributions are added in quadrature to obtain the angular spread of the vertically collimated beam. Thus

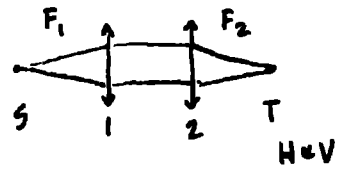
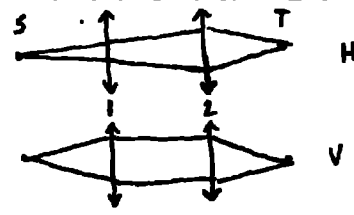
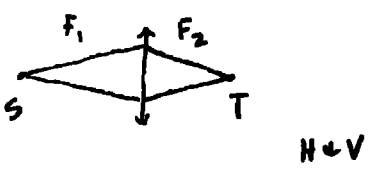
$$\delta \theta = \sqrt{\delta \theta_p^2 + \delta \theta_v^2} \quad . \quad (12)$$

If $\delta \theta$ is less than ω_R , the crystal rocking curve width, then high photon throughput at crystal-limited resolution is obtained. The ratio $\omega_R/\delta \theta$ for this configuration is tabulated in Table II as a "Figure of Merit", (FOM).

Although this section discusses the x-ray optical configuration in which the first mirror collimates both horizontally and vertically (Case I in Table II), two other configurations were considered: (i) two mirrors with the first mirror for vertical collimation through the monochromator and the second mirror to focus the horizontally divergent beam on target (Case II in Table II) and (ii) a single mirror that focuses on target through the monochromator (Case III in Table II). In either instance, the focusing mirror approximates an ellipsoid rather than a paraboloid (See Heald and Hastings). Case III was not chosen because of its poor figure of merit, i.e., $\delta \theta$ is much greater than the crystal rocking curve widths ω_R over a large portion of the energy range. This gives poor x-ray throughput and hence, low flux on target. Even though it has the best figure of merit, Case II was not chosen because the

TABLE II

POSSIBLE MIRROR CONFIGURATIONS

S C H E M A T I C	CASE I		CASE II		CASE III	
						
	bent cylinder M_1	bent cylinder M_2	bent flat M_1	bent cylinder M_2	bent cylinder M_1	No M_2
$F_1 - m$	10		10	$H - \infty$ $V - 15$	10	---
$F_2 - m$	∞	10	∞	$H - 6$ $V - 6$	10	---
$R_s - m$.244	.244	∞		.122	---
$R_m - m$	1636	1636	1636		818	---
$L_v - m$.41	.41	.41	.41	.41	---
$L_H - m$.10	.10	0	.54	.20	---
$L - m$.51	.51	.41	.95	.61	---
$\Delta_s - m$	1.27×10^{-3}	1.27×10^{-3}	0		2.56×10^{-3}	---
$\Delta_m - m$	20.1×10^{-6}	20.1×10^{-6}	20.1×10^{-6}		5.68×10^{-6}	---
$\delta\theta_v$	53×10^{-6} 11.6 arc sec	---	11.6 arc sec	---	11.6 arc sec	---
$\delta\theta_{p,e}$	81.8×10^{-6} 16.9 arc sec	---	0	---	103 arc sec	---
$\delta\theta$	20.5 arc sec	---	11.6 arc sec	---	104 arc sec	---
FOM 0.8 keV Mica(001)	>1	---	>1		>1	---
2 keV Mica(001)	1	---	>1		0.2	---
7 keV Si(111)	.58	---	1	---	0.1	---

second mirror must be nearly 1m long to collect the horizontal divergence. Similar calculations for Case I were also carried out for a second mirror with 7m focal length rather than 10m. Given that there is enough building space for a slightly longer beam line and that procurement and operating costs will be lower with identical mirrors, this alternative was also rejected.

Another significant question to be addressed is whether the absorbed SR flux is sufficient to distort the optical figure. This can be done very conservatively through calculations based on very simplistic assumptions. W_A , the flux absorbed by the mirror can be expressed as

$$W_A = \int_0^{\infty} \frac{dW}{d\varepsilon} (1 - R_\varepsilon) d\varepsilon , \quad (13)$$

where $\frac{dW}{d\varepsilon}$ is the SR energy flux per unit energy interval (See Fig. 5) and R_ε is the reflectivity at ε . This can be approximated by

$$W_A = \left[f (1 - \bar{R}) + (1 - f) \right] \frac{dp}{dA} , \quad (14)$$

where \bar{R} is the average reflectivity below ε_0 , the mirror cutoff energy (see Fig. 6) and f is the fraction of SR flux below ε_0 (see Fig. 4). At 3.4 GeV and 60 mA, we obtain $W_A = .27 \text{ W/cm}^2$. For 3.0 GeV and 100 mA, we obtain $W_A = .22 \text{ W/cm}^2$.

Quartz has relatively poor thermal conductivity, so we make the conservative assumptions that the mirror is flat, that all heat loss is radiative and that the entire mirror equilibrates with a longitudinal surface temperature profile determined by the spatial distribution of SR flux absorbed by the

mirror i.e., there is no thermal gradient perpendicular to the mirror surface. This distribution can be approximated as a Gaussian which peaks at the center of the mirror and which has a full width at half maximum G given by

$$G = \frac{Z}{\theta E}. \quad (15)$$

At 3.4 GeV, $G = 12$ cm; at 3.0 GeV, $G = 13.6$ cm.

The surface temperature of the mirror is given by

$$T = \sqrt[4]{\frac{W_A}{\sigma}} \quad - \text{ } ^\circ\text{K} \quad (16)$$

where $\sigma = 5.7 \times 10^{-12} \text{ W/cm}^2 \text{ } ^\circ\text{K}^4$ is the Stefan-Boltzman constant. At the center of the mirror we obtain $T = 467^\circ\text{K}$ while at 12 cm from the center $T = 388^\circ\text{K}$.

Next we estimate how much the mirror will expand at these locations. From this we can calculate the small change in angle which takes place naturally as a result of non-uniform thermal expansion. For this, we assume that at each horizontal location, the temperature is uniform through the mirror, i.e., the temperature gradient extends along the surface of the mirror. The height difference is

$$\Delta h = h_0 \alpha \Delta T \quad (17)$$

where h_0 is the thickness of the mirror (5.5 cm), $\alpha = 0.4 \times 10^{-6}/^\circ\text{C}$ is the coefficient of thermal expansion and ΔT is the difference in temperatures at

the two locations. Substituting in (17) we obtain $\Delta h = 163 \times 10^{-6} \text{ cm}$. Thus the approximate change in angle from thermal expansion is $\sim 169 \times 10^{-6} / 12 = 13.6 \text{ } \mu\text{rad} = 2.8 \text{ arc sec}$. This should not adversely affect mirror performance even though it will be uncooled. This conclusion is consistent with experience at SSRL where quartz mirrors on bending magnet beam lines are not cooled.

The final consideration deals with the degree of precision required to control the mirror. This can be established from inspection of Eqs 5 and 6, which can be written as

$$R_s = 2 F_1 \sin \theta \quad (6a)$$

and

$$R_m = 2 F_1 \sin \theta \quad (6b)$$

Differentiating and adding relative uncertainties in quadrature gives:

$$\frac{\Delta F_1}{F_1} = \sqrt{\left(\frac{\Delta R_s}{R_s} \right)^2 + (\cot \theta \Delta \theta)^2} \quad (18a)$$

$$\frac{\Delta F_1}{F_1} = \sqrt{\left(\frac{\Delta R_m}{R_m} \right)^2 + (\cot \theta \Delta \theta)^2} \quad (18b)$$

Here we have assumed that the two curvatures collimate or focus (for a collimated beam) independently of each other. Now $\theta = 12.2 \times 10^{-3} \text{ rad}$ and $\cot \theta \approx 1/\theta \approx 81$. Thus we can safely ignore the $\Delta R/R$ terms to obtain

$$\frac{\Delta F_1}{F_1} \approx 81 \Delta \theta \quad (19)$$

We conclude that to obtain good collimation or focusing a premium must be placed on precise angular positioning. This is also apparent from another straightforward geometrical consideration. The direction of the beam should be controllable so that the focal spot on target is within ± 0.1 mm of the desired vertical location. This is given by

$$\Delta y = F_1 \cdot \Delta 2\theta \quad (20)$$

Substituting $\Delta y = 0.1$ mm, we obtain $\Delta\theta = 50 \mu r = 10$ arc sec.

Now the mirror is ~ 0.51 m long. Thus the uncertainty in vertical position of one end of the mirror with respect to the other is

$$\Delta y = 0.51 \text{ m} \times 50 \times 10^{-6} \text{ r} = 25 \mu\text{m} = 1 \text{ mil.}$$

This degree of control is not difficult to achieve with very high precision.

Taking the result from Eq. 20 and substituting in Eq. 19, we obtain

$$\frac{\Delta F_1}{F_1} = 81 \times .5 \times 10^{-4}$$

or $\Delta F_1 \cong \pm 40.5 \text{ mm}$

This uncertainty in ΔF_1 is not judged to be very serious because it is smaller than the length of the SR arc source and because the depth of focus for a 10 m focal length mirror is large.

The mirror control presently being designed by H. Hampal and E. Hanson of LLNL has provision for pitch, yaw and roll control as well as for horizontal and vertical displacements, all with precision of $\pm 1 \mu\text{m}$ or smaller. There is also a pneumatically controlled mechanism that can bend the mirror to the correct meridional radius. Table II lists the deflection Δ_m required to obtain a 1628 m radius of curvature.

C. Filters. A filter serves two purposes, first to reduce the VUV radiation flux on the diffraction crystal and second to reduce first order diffraction so that background from higher order diffraction can be subtracted. The former may be quite important when using crystals such as mica and quartz, since these are subject to VUV radiation damage. It is necessary to reduce the first order diffraction intensity when diffraction efficiency for higher orders is large and it is difficult to slightly detune the monochromator to reduce high order diffraction. The usual approach of using filters with K- or L- edges to preferentially absorb high energy photons is not applicable here. This is because the cross sections at energies ϵ and 2ϵ are comparable when an absorption edge falls between ϵ and 2ϵ . For an edge between ϵ and 3ϵ , the cross section at 3ϵ is substantially smaller than at ϵ . Thus, filtration must accomplish the opposite, i.e., preferential transmission of higher energy photons. This can be accomplished with very thin Be or C foils that are several mean-free-paths thick at the first-order energy, and owing to the strong dependence of x-ray absorption cross section on energy ($\sim \epsilon^{-3}$), are less than one mean-free-path for higher order energies.

As an example, let us consider the case of 1 keV first order diffraction. To effectively eliminate these photons but transmit 2 keV and higher energy, the attenuation at 1 keV should be $\sim 10^{-1} - 10^{-2}$. The x-ray mean-free-paths τ of Be and C at 1 keV are $\tau_{\text{Be}} = 9.54 \times 10^{-4}$ and $\tau_{\text{C}} = 2.02 \times 10^{-4}$ cm, respectively. The x-ray transmittances of 4 mean-free-path Be and C foils at 2- and 3- keV are tabulated in Table III.

TABLE III
TRANSMITTANCE AND TRANSMITTANCE RATIOS OF LOW Z FILTERS

A. Beryllium			
ϵ - keV	1	2	3
τ_{ϵ} - cm	$.954 \times 10^{-3}$	7.43×10^{-3}	26.4×10^{-3}
$T = \exp - \frac{4\tau_1}{\tau_{\epsilon}}$.0183	.598	.865
T_{ϵ} / T_1	1	32.6	47.3
B. Carbon			
ϵ - keV	1	2	3
τ_1 - cm	$.202 \times 10^{-3}$	1.45×10^{-3}	4.91×10^{-3}
$T(4 \tau_1)$.0183	.573	.848
T_{ϵ} / T_1	1	31.3	46.3

From Table III it can be seen that favorable transmittance ratios of 30/1 and 40/1 are achievable with low Z filters. Using a greater number of mean-free-paths increases this ratio. Clearly, the actual thicknesses required will depend upon the nature of the experiment and the efficacy of other discrimination methods in both data acquisition and analysis.

It should also be mentioned that with insertion of additional filters in the reflected x-ray beam, the thermal loading in the monochromator will suddenly change. This does not appear to be a problem since the change will be small. It remains to be seen whether performance will be seriously affected even though crystal cooling will be provided. If this turns out to be serious, the x-ray filters should be relocated downstream of the monochromator.

D. Monochromator: The monochromator will be located 13m from the arc source to accept photons reflected 1.4 deg from the horizontal plane. Of some concern is the close proximity of this beam line to the concrete shielding blocks that surround the storage ring. Access to this instrument can only be from one side. Because the ultimate resolution of a monochromator is determined by the characteristics of available crystals, the decision was made to purchase a commercially available ultra-high vacuum double crystal monochromator, and eliminate the expense of designing our own monochromator. The instrument selected is a modification of one designed by Hunter, et al, [Nucl. Instrum. and Meth. 195, 141 (1982)]. Several of these have been manufactured for other synchrotron beam lines. In this modified version, only crystals and not gratings are used for monochromatization. This device covers a range of 8 deg to 70 deg in Bragg angle with ± 5 arc sec angular accuracy with ± 2 arc sec precision. There is provision to retrofit a commercially available laser interferometer system that would allow an angular accuracy of ± 1 arc sec. The crystals are arranged non-dispersively as shown in Fig. 10 to eliminate large rotation of the experiment chamber located ~ 13 m downstream of the monochromator. In this configuration, the first crystal (water cooled) rotates and the second crystal rotates and translates to maintain a fixed beam

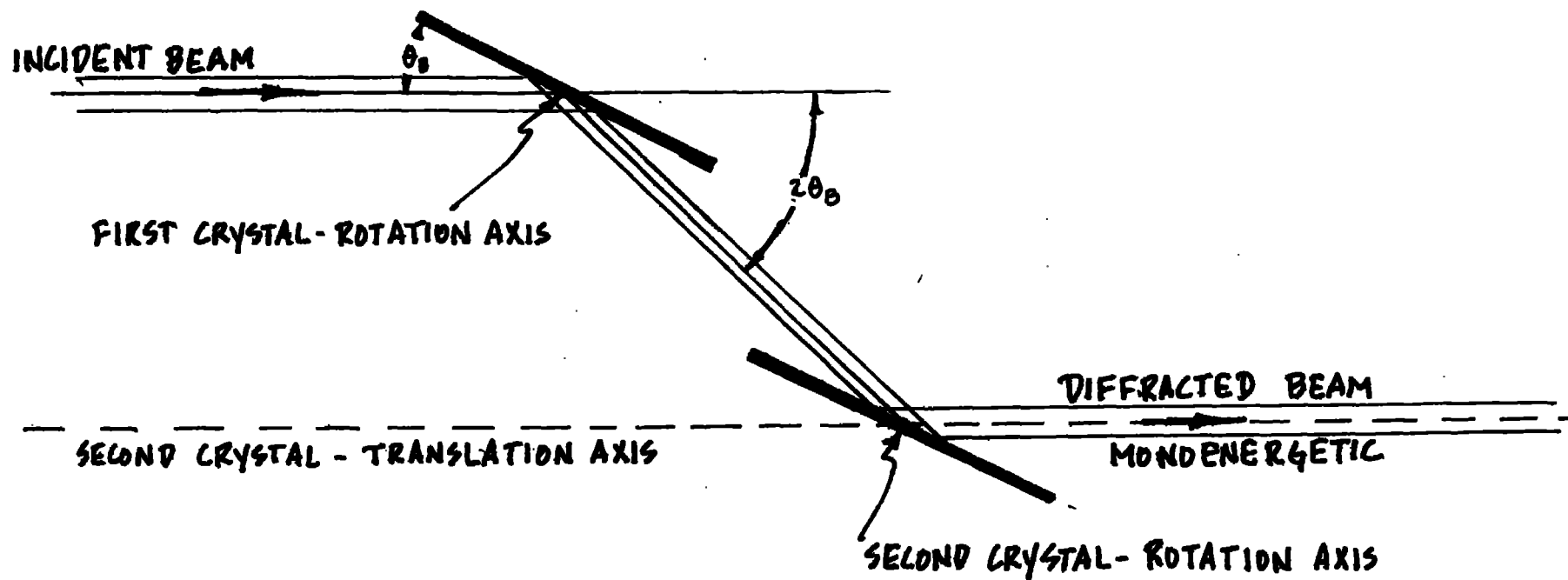


FIG. 10. DOUBLE CRYSTAL CONFIGURATION

position on target. The diffraction crystals can be as large as 5 cm x 7 cm, which is more than enough to fully cover the projected dimensions of the reflected photon beam. Water cooling sufficient to dissipate 100W will be provided, and the monochromator will operate in the 10^{-9} Torr pressure range. Several other monochromators considered did not have all of the features mentioned above and were judged to be inappropriate for our needs.

Table IV lists possibilities for crystals, the energy range covered in first order and relative stability in intense synchrotron radiation fluxes. Rocking curve widths for some of these are shown in Fig. 11. The significant issues then become those of selecting appropriate crystals to adequately cover the energy range, and of assuring that these are not adversely affected by thermal loads. It is clear that the desired energy range can be covered. We now address the question of thermal loading.

The flux reflected by the mirror and incident on the first crystal (see Eq. 13) can be approximated as

$$W_C = R f W_1 \quad (17)$$

For $E = 3.4$ GeV, we obtain $W_C = 8W/cm^2$.

Since the photons are low energy, we conservatively assume all absorption is at the crystal surface. Then the temperature gradient introduced in the crystal is related to the incident flux by the expression

$$W_C = k \frac{dT}{dx} \quad (18)$$

TABLE IV
ENERGY COVERAGE OF POSSIBLE DIFFRACTION CRYSTALS

Crystal/Plane/ Composition	$2d$ - Å	$h\nu(\theta_B=70^\circ)$ - eV	$h\nu(\theta_B=8^\circ)$ - eV	Remarks/References
β -Alumina (0002) Na Al ₁₁ O ₁₇	22.49	586	3959	Relatively stable when annealed. (1)(2)
MICA - (001) KAl ₃ Si ₃ O ₁₂ H ₂	19.91	663	4475	Some success w/S.R. low reflectivity (1)(3)
SYNTHETIC MICA (001)-KMg ₃ AlSi ₃ O ₁₀ F (THERMICA)	19.93	662	4470	Good neutron monochromator. (3) Refl. higher than MICA Resoln. higher than MICA
BERYL - (10 $\bar{1}$ 0)	15.96	826	5581	Very expensive (1)(2)
GYPSUM (020) CaSO ₄ · 2H ₂ O	15.17	870	5873	Poor in vacuum
MoS ₂ (0001)	12.30	1073	7242	(7) (8)
YB ₆₆ (400)	11.76	1121	7575	New material (2)
α - SiO ₂ (10 $\bar{1}$ 0)	8.512	1550	10470	Damages (2)
InSb (111)	7.481	1763	11910	(2)
Ge (111)	6.533	2020	13640	(5) Stable; perfect
Si (111)	6.271	2103	14210	(6) Stable; perfect
Ge (220)	3.392	3305	22710	(5) Stable; perfect
Si (220)	3.840	3436	23200	(6) Stable; perfect Very high resolving power
VERY LOW ENERGY				
MULTILAYERS	SELECTABLE	80	500	(7) Stable; relatively poor resolution.
dioctadecyladipate	90.55	146	984	Pressure <4x10 ⁻⁸ torr organic; (8)

TABLE 4 (continued)

Table References

- (1) Nucl. Instrum. and Meth. 195, 133 (1982).
- (2) Nucl. Instrum. and Meth. 195, 115 (1982).
Nucl. Instrum. and Meth. 208, 333 (1983).
- (3) Rev. Sci. Instrum. 30, 269 (1959).
- (4) X-Ray Spectrometry 4, 74 (1975).
- (5) Arkiv for Fysik 23, 81 (1962).
- (6) Arkiv for Fysik 22, 535 (1962).
- (7) Optical Engineering 23, 667 (1984).
Optical Engineering 24, 197 (1985).
- (8) Phys. Stat. Sol. 32, K23 (1975).
- (9) Z. Agnew, Phys. 24, 129 (1968).

General References

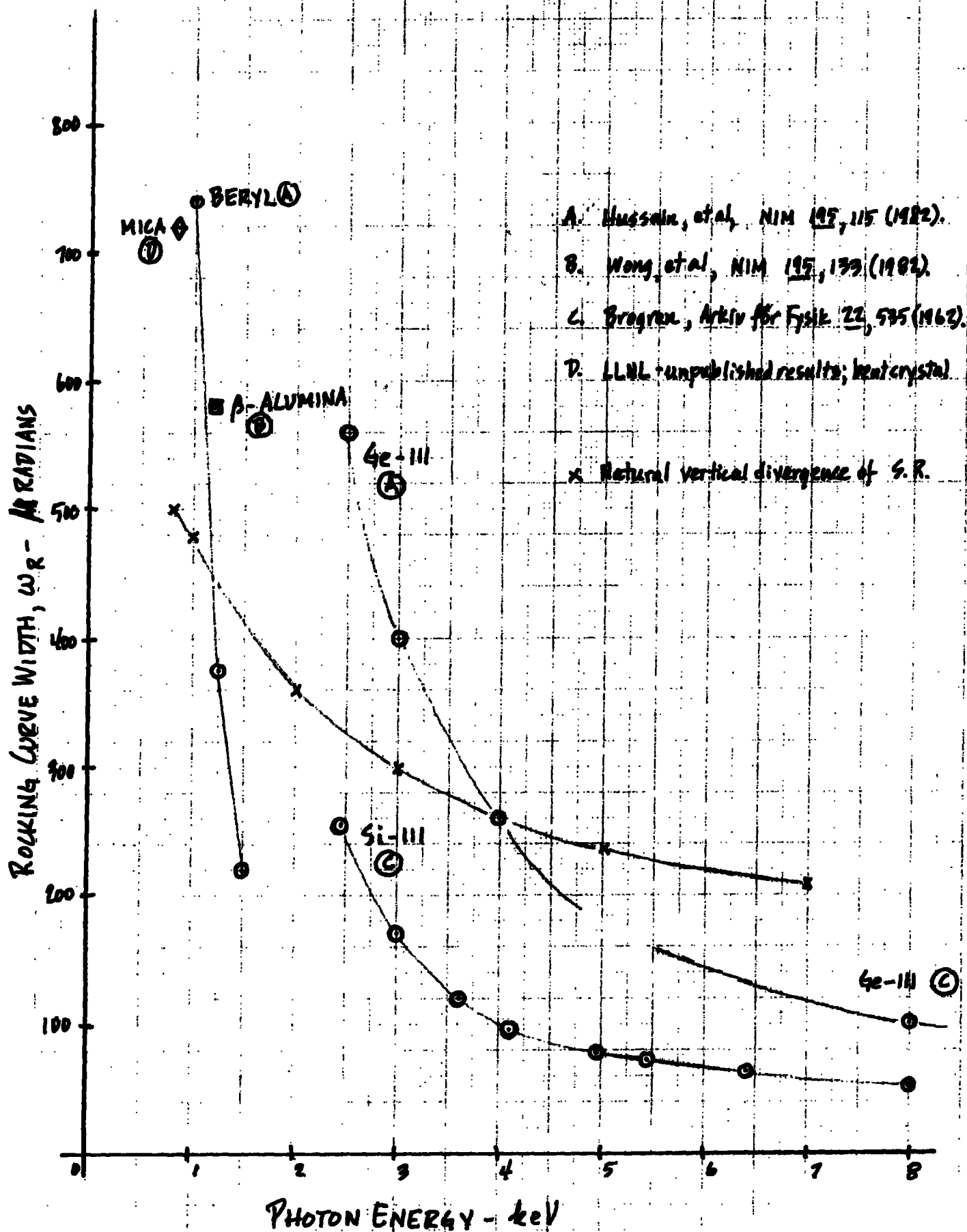
International Tables for X-Ray Crystallography, The Kynoch Press,
Birmingham, England (1962) p.79ff.

N.G. Alexandropoulos and G.C. Cohen, Applied Spectroscopy 28, 155 (1974).

Standard X-Ray Diffraction Powder Patterns, NBS Circular 539.

FIG. 11

ROCKING CURVE WIDTHS vs. PHOTON ENERGY



where k is the coefficient of thermal conductivity. For poor thermal conductors such as quartz and mica, where $k \approx 10^{-2} \frac{\text{W}}{\text{cm } ^\circ\text{C}}$, we obtain a thermal gradient of $\frac{\Delta T}{\Delta X} \sim 10^3 \text{ } ^\circ\text{C/cm}$.

Clearly the crystals must be very thin ($\sim 10^{-2} \text{ cm}$) to avoid significant change in lattice parameters. The situation is not nearly as bad for Ge or Si where $k \approx 1 \text{ W/cm } ^\circ\text{C}$, and rather thick crystals could be used. Since most diffraction occurs within the first 10^3 - 10^4 crystal planes, there should be no problem achieving high diffraction efficiency with thin crystals. Good thermal contact, however, will be extremely important. The crystals will probably have to be soldered on to a high conductivity substrate to accomplish this.

It is worthwhile to briefly consider how thermal loading affects energy. We do this by calculating the expansion of the crystal. Again we consider the case for mica which has a thermal expansion coefficient $\alpha = 18 \times 10^{-6}/^\circ\text{C}$. The fractional change in $2d$ spacing as a function temperature, is equal to $\alpha\Delta T$. Thus for $\sim 10^2$ $^\circ\text{C}$ surface temperature rise, again conservatively assuming that thermal contact is a factor of 10 poorer than ideal, we obtain

$$\frac{\Delta(2d)}{2d} = 1800 \times 10^{-6} \approx 2 \times 10^{-3}$$

From Bragg's equation ($n\lambda = 2d \sin \theta_B$), we have for fixed θ_B ,

$$\frac{\Delta E}{E} = \frac{\Delta\lambda}{\lambda} = \frac{\Delta(2d)}{2d} = 2 \times 10^{-3}$$

This amounts to a 2 eV energy shift at 1000 eV. In some experiments this could be serious. However since the rocking curve width is smaller than 2 eV the desired energy can be selected by setting the second crystal at the correct Bragg angle and adjusting the angle of the first crystal for maximum intensity. The monochromator has provision for this kind of correction.

It should also be pointed out that the monochromator controls provided by the vendor will interface with an LSI 11/23 that is the central element of the control and data acquisition system of Beam Line VIII-B.

E. Second Mirror: This mirror focuses the collimated monochromatic beam on target, 10m downstream. It and its control mechanism located 15m from the source will be the same as those for the first mirror to help reduce costs. Obviously, heat loading will be no problem. E. Berglin of LLNL used the ray tracing code SHADOW (developed by F. Cerrina at Wisconsin) to calculate the optical properties of this branch line for the double mirror design discussed herein. The results showed a well defined beam spot of unit magnification at 10m from the second mirror.

The focal length of this mirror can be varied. This can be seen from Eqs. 5 and 6. For example, to obtain a longer sagittal focal length for a fixed R_g (ground into the mirror), θ must decrease. On the other hand to obtain a longer meridional focal length with smaller θ , the radius R_M must increase. These operations can be accomplished with the mirror control mechanism.

Thus, the double mirror configuration also offers the additional benefit of operating with multiple end stations. This could prove very valuable in reducing the amount of time lost in setting up experiments.

F. Experiment/Diagnostics Chamber: A standard LLNL multipurpose target chamber was chosen for this component. It has 30 cm height and 60 cm diameter with all metal seals for UHV operation. It has eight side ports and a remov-

able lid for ease of access. This chamber is versatile enough for installation of commercially available UHV multi-axis sample positioners, etc. required for SXR experiments. It is also possible to locate a second chamber in tandem since the focal properties of the second mirror can be adjusted. Suppose a second chamber were located with its center 100 cm further downstream. Then a focal length of 11m would be needed for the second mirror. This is accomplished simply by reducing θ by 10% and increasing R_m by 10%. Of course, the target spot will be displaced vertically because the reflection angle would be smaller. This displacement is given as follows:

$$\Delta y = Z \cdot 2 \Delta\theta \cong 10 \times 2 \times 10^{-3} = 2 \text{ cm.}$$

Several beam monitoring options are also worth considering. The major ones are (1) photon rate, (2) spot size, (3) pulsed time structure and (4) polarization. It is assumed that photon energy and energy resolution are determined in the monochromator from Bragg's law. From Fig. 5, we see that for a 5 mr horizontal fan, the source output is $\sim 3 \times 10^{13} \frac{\text{phot}}{\text{sec} \cdot 0.1\% \text{ B.W.}}$ at 3 GeV and 100 mA. Thus at 1 keV (0.1% BW = 1 eV), the source emits $3 \times 10^{13} \frac{\text{phot}}{\text{sec}}$ in a 1 eV wide energy interval.

Referring to Fig. 6, each mirror reflects $\sim 88\%$ of the incident beam. The reflectivity of each crystal is $\sim 10\%$. Thus there are $3 \times 10^{13} \times .88 \times .1 \times .1 \times .88 = 2 \times 10^{11}$ photons/sec incident on a $\sim 3 \text{ mm}^2$ target spot.

(1) The number of photons/sec incident on target can be measured with a standard Be cathode X-ray diode detector. Nominal sensitivity at 1 keV is $\sim 10^{-20} \text{ C/keV}$. Thus a current of $2 \times 10^{-9} \text{ A}$ will be generated, and this can be measured with high accuracy. More sensitive photocathodes such as CsI could be considered if this proves necessary.

(2) Beam spot dimensions can be monitored using standard phosphors which are suitable for ultra-high-vacuum operation. More accurate measurement of beam dimensions can be obtained with a scanning slit or oscillating wires that emit photoelectrons.

(3) Pulsed time structure of a monoenergetic beam may prove more difficult to measure. The peak x-ray rate is $\sim 600\times$ greater than average, or 1×10^{14} phot/sec. This could be measured with a streak camera that is synchronized to sweep with the synchrotron beam. Alternatively the peak current in the XRD detector would be 10^{-6} A. Use of a fast amplifier with gain of 100 and a 50Ω system would give signal amplitude of 5mV. This can be easily recorded on an oscilloscope.

(4) We will discuss the polarization measurement in the context of a proposed x-ray scattering experiment.

It would be instructive to work through such an experiment to see how beam monitoring, etc. would be accomplished. We wish to measure the scattering of x-rays by low Z atoms. Both coherent and incoherent scattering contribute. Since the incident energy is ~ 1 keV, the Compton defect is quite small (~ 2 eV at 90° scattering angle) and therefore cannot be resolved with a small, thin window proportional counter. It should be possible to do this with a crystal spectrometer, but as will be seen, the data rate would be quite low.

From experiments done at LLNL, we know that the scattering efficiency of a 1-mean-free-path scatterer is $\sim 10^{-5}$ /sr at 90° scattering angle. Thus

for a detector with 30% efficiency and subtending 10^{-3} sr, we would expect a count rate of $2 \times 10^{11} \times 10^{-5} \times 0.3 \times 10^{-3} = 6 \times 10^2$ /sec. A crystal monochromator, has $\Delta\Omega \approx 10^{-5}$ sr and reflectivity of 10^{-1} . Thus, with a position sensitive detector (to record Bragg angle) we expect a count rate of $2 \times 10^{12} \times 10^{-5} \times 10^{-5} \times 10^{-1} \times 0.3 = 0.6$ /sec. Both experiments would be feasible, even with much thinner scatterers. Beam monitoring would take place with an XRD located behind the scatterer.

It should be noted that the x-ray flux contribution from higher orders can easily be measured with a gas proportional counter viewing the scatterer. Note also that scattering at 90 deg preserves polarization. Thus, the degree of polarization can be determined by rotating the detector azimuthally about the beam axis so that the detector measures scattered photons horizontally and vertically. The degree of horizontal polarization is given by

$$P_H = \frac{C_V - C_H}{C_V + C_H}$$

where C_V and C_H are count rates with the detector vertical and horizontal, respectively.

As a final comment, we note that at 1 keV, the x-ray throughput is roughly 10^{-2} and is dominated by the reflectivity of mica or synthetic mica. The reflectivity of Ge and Si are substantially higher (~ 0.7) and throughputs ~ 0.2 are expected with these crystals and two reflections.